Available online at www.sciencedirect.com
SCIENCE DIRECT®
Vision Research 44 (2004) 1857–1867
Vision Research
www.elsevier.com/locate/visres

A paraxial schematic eye model for the growing C57BL/6 mouse

Christine Schmucker, Frank Schaeffel *

Section of Neurobiology of the Eye, University Eye Hospital, Calwerstr. 7/1, 72076 Tuebingen, Germany

Received 19 November 2003; received in revised form 12 March 2004

Abstract

Purpose. The mouse eye has potential to become an important model for studies on the genetic control of eye growth and myopia. However, no data are published on the development of its optical properties. We developed a paraxial schematic model of the growing eye for the most common laboratory mouse strain, the C57BL/6 mouse, for the age range between 22 and 100 days.

Methods. Refractive development was followed with eccentric infrared photorefraction and corneal curvature with infrared photokeratometry. To measure ocular dimensions, freshly excised eyes were immediately frozen after enucleation to minimize distortions. Eyes were cut with a cryostat down to the bisecting horizontal plane, until the optic nerve head became visible. The standard deviations were ±10 μm for repeated measurements in highly magnified videographs, taken in several section planes close to the equator in the same eyes. To evaluate inter-eye and inter-individual variability, a total of 20 mice (34 eyes) were studied, with 3–4 eyes for each of the 9 sampling ages. Schematic eye models were developed using paraxial ray tracing software (OSLO, LT Lambda Research Corporation, and a self-written program).

Results. The measured refractive errors were initially +4.0 ± 0.6 D at approximately 30 days, and levelled off with +7.0 ± 2.5 D at about 70 days. Corneal radius of curvature did not change with age (1.414 ± 0.019 mm). Both axial lens diameter and axial eye length grew linearly (regression equations: lens, 1619 μm +5.5 μm/day, $R = 0.916$; axial length, 2899 μm +4.4 μm/day, $R = 0.936$). The lens grew so fast that vitreous chamber depth declined with age (regression equation: 896 μm −3.2 μm/day, $R = 0.685$). The radii of curvature of the anterior lens surface increased during development (from 0.982 mm at day 22 to 1.208 mm at day 100), whereas the radii of the posterior lens surface remained constant (−1.081 ± 0.054 mm). The calculated homogeneous lens index increased linearly with age (from 1.568 to 1.605). The small eye artifact, calculated from the dioptric difference of the positions of the vitreo-retinal interface and the photoreceptor plane, increased from +35.2 to +39.1 D, which was much higher than the hyperopia measured with photorefraction. Retinal image magnification increased from 31 to 34 μm/deg, and the f/number remained $\leqslant 1$ at all ages, suggesting a bright retinal image. A calculated axial eye elongation of 5.4–6.5 μm was sufficient to make the schematic eye 1 D more myopic.

Conclusions. The most striking features of the mouse eye were that linear growth was slow but extended far beyond sexual maturity, that the corneal curvature did not increase, and that the prominent lens growth caused a developmental decline of the vitreous chamber depth.

1. Introduction

Myopia is one of the most common ocular disorders in humans. Its incidence is approximately 25% of most Western populations and reaches more than 80% in Asian school children (Rajan et al., 1998). Even though there is considerable experimental (i.e. Gwiazda et al., 2003) and epidemiological evidence (i.e. Saw, 2003) from human studies that environmental factors play a role, a number of studies demonstrate a strong genetic influence. School-age children with two myopic parents are far more likely to be myopic (62%) than children with one or no myopic parent (19% and 24%, respectively) (i.e. Thorn, Grice, Held, & Gwiazda, 1998). Analyses of extended multi-generation families provide also convincing evidence of inheritance (i.e. Pacella et al., 1999).

Although low degrees of myopia are generally innocuous, higher degrees of myopia may lead to permanent visual impairment and blindness since high myopia is associated with a higher risk of additional ocular disorders such as glaucoma (Wu, Nemesure,

* Corresponding author. Tel.: +49-7071-2980739; fax: +49-7071-295196.
E-mail address: frank.schaeffel@uni-tuebingen.de (F. Schaeffel).
URL: http://www.uak.medizin.uni-tuebingen.de/frank/.

0042-6989/$ - see front matter © 2004 Elsevier Ltd. All rights reserved.
doi:10.1016/j.visres.2004.03.011

& Leske, 1999) cataract (Wu et al., 1999), retinal degeneration, peripheral retinal changes and retinal detachments (Krumpaszky, Haas, Klauss, & Selbmann, 1997).

While the influence of environmental factors can be readily studied in both animals and humans, the mapping of loci that include genes for the control of eye growth and myopia is more challenging (Schaeffel, Simon, Feldkaemper, Ohngemach, & Williams, 2003). Zhou and Williams (1999a) used quantitative trait loci (QTL) analysis in mice and Young et al. (1998) used transmission disequilibrium tests (TDT) in humans. Even though several animal models (mainly chick, tree shrew, marmoset and macaque) have been established, their limitations are that information on the genome, transcriptome, and proteome may be incomplete. This is different for the mouse which represents the most widely used mammalian model for human diseases. Its genome has been largely sequenced (Mouse Genome Sequencing Consortium, 2002), and many knockout models are available. Furthermore, the mouse is readily available, grows rapidly, and can be easily bred, although the highly inbred laboratory strains preclude selective breeding i.e. for high susceptibility to myopia. The mouse eye growth responds with deprivation myopia when it is covered with diffusers (Schaeffel & Burkhardt, 2002) or lid sutured (Tejedor & de la Villa, 2003), although the responses are less reliable than in other animal models of myopia (Schaeffel, Burkhardt, Howland, & Williams, 2004). Due to the lack of appropriate technologies to measure ocular dimensions, axial length data are either missing (Schaeffel & Burkhardt, 2002) or have limited reliability because the histological techniques used for the measurement are not sensitive enough (Tejedor & de la Villa, 2003). Also, the axial length changes calculated from schematic eye models of the adult mouse (Remtulla & Hallett, 1985) were smaller than the measured changes by an order of magnitude (Tejedor & de la Villa, 2003) or even more (Beuerman, Barathi, Weon, & Tan, 2003). A schematic eye model for the growing eye of the most common laboratory mouse strain (C57BL/6) would provide baseline data against which data from experimentally myopic animals could be compared. Therefore, in this paper, a paraxial schematic eye model was developed for the age range between 22 and 100 days, using in vivo infrared photoretinoscopy and photokeratometry, and frozen sections of excised eyes.

2. Material and methods

2.1. Animals

Black C57BL/6 wildtype mice were obtained from Charles River, Sulzfeld, Germany, and bred in the animal facilities of the Institute. A maximum of six to eight animals were housed in standard mouse cages under 12 h light/dark cycle. Illuminance on the cage floor was about 500 lux. The treatment of the mice was approved by the University commission for animal welfare (reference AK3/02) and was in accordance with the ARVO resolution for care and use of laboratory animals.

2.2. Infrared photoretinoscopy

Refractive state and pupil size of the mice were recorded by eccentric infrared photoretinoscopy (the Power Refractor) as described by Schaeffel et al. (2004). In brief, the slopes of the brightness distributions in the pupil were automatically determined in the digital video images with 25 Hz sampling rate using an image processing computer program written by Schaeffel. The brightness slopes were converted into refractive errors, using a factor that was determined in prior calibrations with trial lenses (Schaeffel et al., 2004). Infrared light had the advantage that the animals were not aware of the measurements, and that the pupil size remained large. A previous study (Schaeffel et al., 2004) showed that mice could be refracted with a standard deviation from several repeated measurements of ±2.5 D. To measure refractions, the mice were not anesthetized and only slightly restrained by grabbing their tails. No cycloplegia was necessary since the room was kept dark. Pupil sizes were approximately 2 mm under these conditions but dropped to less than 1 mm when the room light was turned on (Pennesi, Lyubarsky, & Pugh, 1998).

2.3. Infrared photokeratometry

Corneal radius of curvature was measured in vivo by infrared photokeratometry in 11 mice at the age of 35, 58 and 75 days. Mice were anesthetized with an intraperitoneal injection of 0.1–0.2 ml of a mixture of 1.2 ml 10% ketamine hydrochloride, 0.8 ml 2% xylazine hydrochloride and 8.0 ml sterile saline. After carefully positioning the eye, eight infrared light-emitting diodes (LEDs) arranged in a circle of a diameter of 298 mm created 8 Purkinje images on the cornea (Fig. 1). The positions of these reflexes were recorded by an infrared light sensitive video camera equipped with a 210 mm lens and several extension rings, resulting in a highly magnified video image (about 80 pixel/mm). Calculation of corneal radius of curvature from the positions of the infrared light reflexes on the cornea was done following prior calibration and linear extrapolation from measurements on two ball bearings with known radii (3.15 and 5.50 mm). The standard deviation from repeated measurements of the radii of curvature in the ball bearings was ±0.02 mm. In addition to the in vivo measurements, corneal radii of curvature were also determined in frozen sections. Both measurements did not differ by more than 0.08 mm, even though these

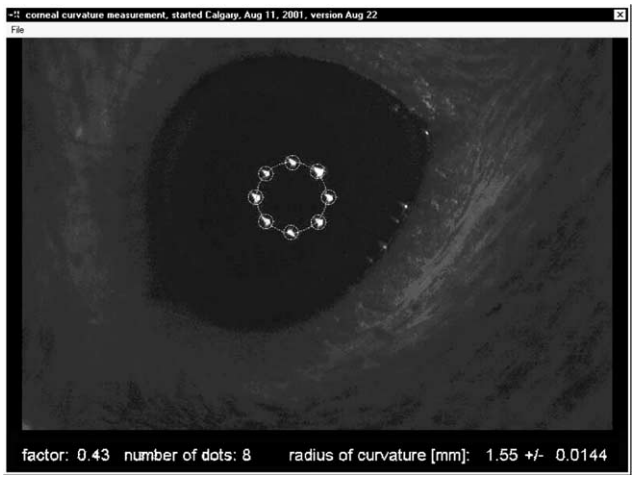

Fig. 1. Screen dump of the C++ program that located the first Purkinje images created by a circular arrangement of eight infrared LEDs on the corneal surface in a highly magnified video image of the mouse eye in vivo. The radius of curvature was automatically determined by the program, based on a prior calibration with ball bearings of known radius. Ten measurements acquired in 0.4 s had a standard deviation of the radii of curvature of about 15 μm.

differences reached significance with the large number of samples (in vivo keratometry: 1.493 ± 0.080 mm; frozen sections: 1.414 ± 0.019 mm; $p < 0.001$).

2.4. Frozen sections

Freshly excised globes were placed on the cooled metal platform of the cryostat with defined orientation and immediately embedded in freezing medium (TissueTec™) at −20 °C. Once completely frozen after about 20 min, the globes were sectioned parallel to the horizontal plane until the maximal equatorial diameter was reached and the optic nerve head became visible. Subsequently, three videographs with high magnification (about 150 pixel/mm achieved with a 135 mm lens with several extension rings) were taken of the frozen block at three different planes with 36 μm distance in depth. After digitalization of the video frames, ocular dimensions and radii of curvature of the optical surfaces were determined, using Adobe Photoshop™. Radii of curvature of cornea, lens and retina were calculated from the equation $r = y^2/(2 \times s) + s/2$ with $r =$ radius of curvature, $s =$ sagitta of the chord, $y =$ any chord (Fincham & Freeman, 1974). In each videograph, three measurements were taken at different distances from the optical axis.

No corrections were made for volume artifacts which were previously shown to be very small (Chaudhuri, Hallett, & Parker, 1983). Furthermore, both Charman and Tucker (1973) and Sivak (1974) observed no significant changes in the dimensions of the anterior chamber or crystalline lens following freezing eyes in the cryostat.

The data on ocular dimensions were plotted versus age and linear regressions were fit to analyze changes over time. Significant changes over time were recognized by significant correlation coefficients. Since no correlation was found between the axial lengths of both eyes in animals of the same age group (Schaeffel et al., 2004), eyes were treated as independent samples even if they originated from the same animal.

2.5. Paraxial ray tracing and schematic eyes

Schematic eyes were developed using both the "OSLO" paraxial ray tracing program (LT Lambda Research Corporation) and a ray tracing program written by Schaeffel and Howland (1988). The programs were tested against each other and were found to produce identical results. Radii of curvatures and positions were taken from the frozen sections. Refractive indices of the optical media in the mouse were taken from the literature for a wavelength of 655 nm (cornea 1.4015, aqueous 1.3336 and vitreous 1.3329, Remtulla & Hallett, 1985). The refractive index of the retina of 1.351 was taken from a study on the rat eye (Hughes, 1979). The equivalent homogeneous refractive index of the lens was calculated by matching the refractive state of the model eye to the refractions measured with infrared photoretinoscopy. A limitation was then that nothing could be said about off-axis imagery, since this depends heavily on the nature of the refractive index gradient in the lens. As in other studies, the calculated equivalent homogeneous refractive index of the lens of the schematic eye was higher than what is possible for biological materials (<1.55, Hughes, 1979).

In the present study the position of the retinal pigment epithelium was assumed to be coincident with the photoreceptor plane, as it could be easily identified in the frozen block. The theoretically expected small eye artifact was calculated from the dioptric differences between the photoreceptor plane and the retino–vitreal interface (Glickstein & Millodot, 1970). The paraxial eye model also permitted us to calculate the developmental changes in image brightness and image magnification.

3. Results

3.1. Development of refractive state and pupil size

The refractive development of the mice, as measured with infrared photoretinoscopy, is shown in Fig. 2A. The least hyperopic refractions were measured at day 32 (mean refraction ± SD: $+4.1 \pm 0.6$ D). Hyperopia increased and reached a peak at around day 55 ($+9.8 \pm 2.7$ D). From day 70, the measured refractions became stable and levelled off at $+7.0 \pm 2.5$ D. Developmental changes in pupil size are shown in Fig. 2B. Pupil

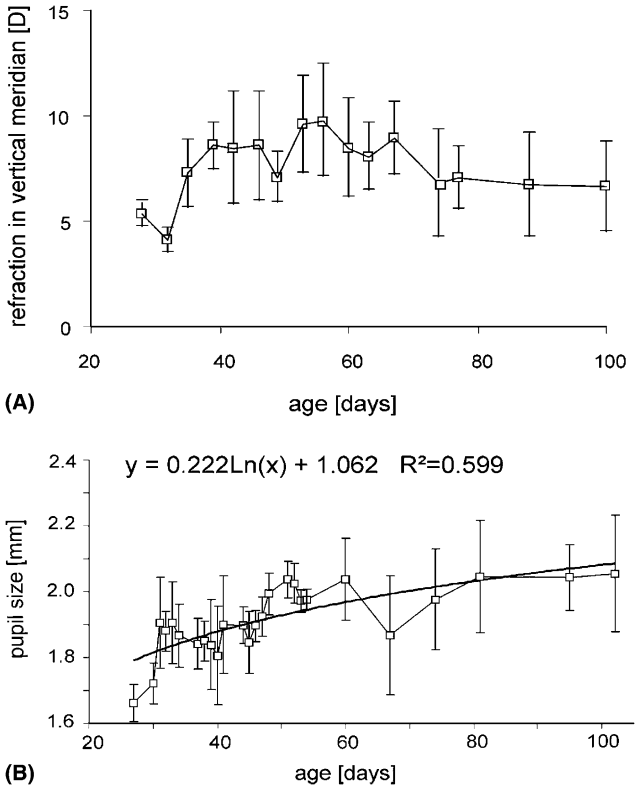

Fig. 2. (A) Average development of refractive state (mean ± SD) in three C57BL/6 mice measured by infrared photoretinoscopy. No correction was made for a small eye artifact (see Section 4). Note that with this technique, the mice reach a final refraction (+7.0 ± 2.5 D) after 70 days of age. (B) Growth of the pupils of the mice over the first 100 days. Error bars denote standard deviations.

diameter increased from about 1.78 mm at day 25 to 2.08 mm at day 100.

The appearance of the photoretinoscopic reflexes in the pupils suggested considerable amounts of aberrations in the eyes since ring-shaped areas of higher brightness were visible (Fig. 3) which are not detectable in eyes with high optical quality like those of humans or birds. However, since such brightness distributions were already observed by Remtulla and Hallett (1985) and were present in most of the mice in our study, it is unlikely that the underlying ocular aberrations were random. Rather, the presence of the ring-shaped areas with higher brightness may indicate that the lenses were multifocal, similar to what has been described for fish eyes by Kroger et al. (1999).

3.2. Growth of the ocular dimensions

Examples of frozen sections of two mouse eyes are shown for the ages of 23 days and 85 days in Fig. 4A and B, respectively. Note that the lens increased considerably in size, resulting in a decline of the vitreous chamber depth.

Growth curves of corneal thickness, anterior chamber depth, axial lens thickness, vitreous chamber depth, retinal thickness and axial length are shown in Fig. 5. The growth of the different components could be described by linear regressions. Exponential or logarithmic functions did not increase the quality of the fits. Accordingly, there was no indication of a reduction or saturation of the eye growth rates over the first 100 days which is surprising, given that mice are mature at the age of about 50 days. This observation is in line with Zhou and Williams (1999b) who state that "eye growth continues long after sexual maturity is reached at 40–60 days of age". Axial length (the sum of corneal thickness,

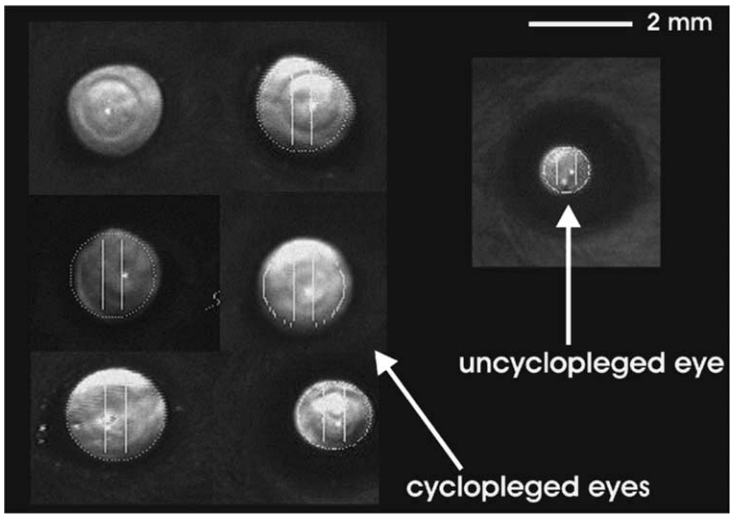

Fig. 3. Brightness distributions observed in the pupils of mice during infrared photoretinoscopy. Left colum: Appearance of the pupils in 6 animals under cycloplegia (pupil sizes about 2 mm). Right: Appearance of a pupil without cycloplegia, refracted at about 2 lux ambient illumination (pupil size about 1 mm). The ring-shaped areas of different brightness in some eyes may reflect the presence of multifocal lenses as observed by Kroger, Campbell, Fernald, and Wagner (1999) in fish eyes.

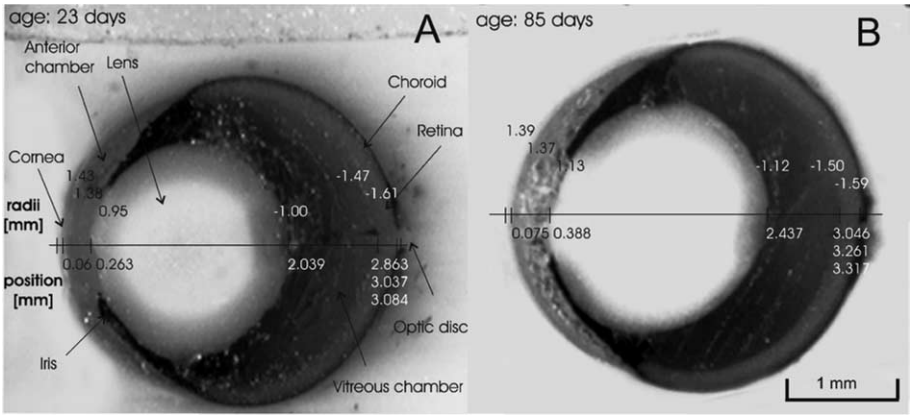

Fig. 4. Frozen sections of mouse eyes at two different ages. Radii of curvature (labelled above the optical axis) and positions (labelled below the optical axis) of the optical surfaces were measured in these videographs and used to construct the schematic eyes.

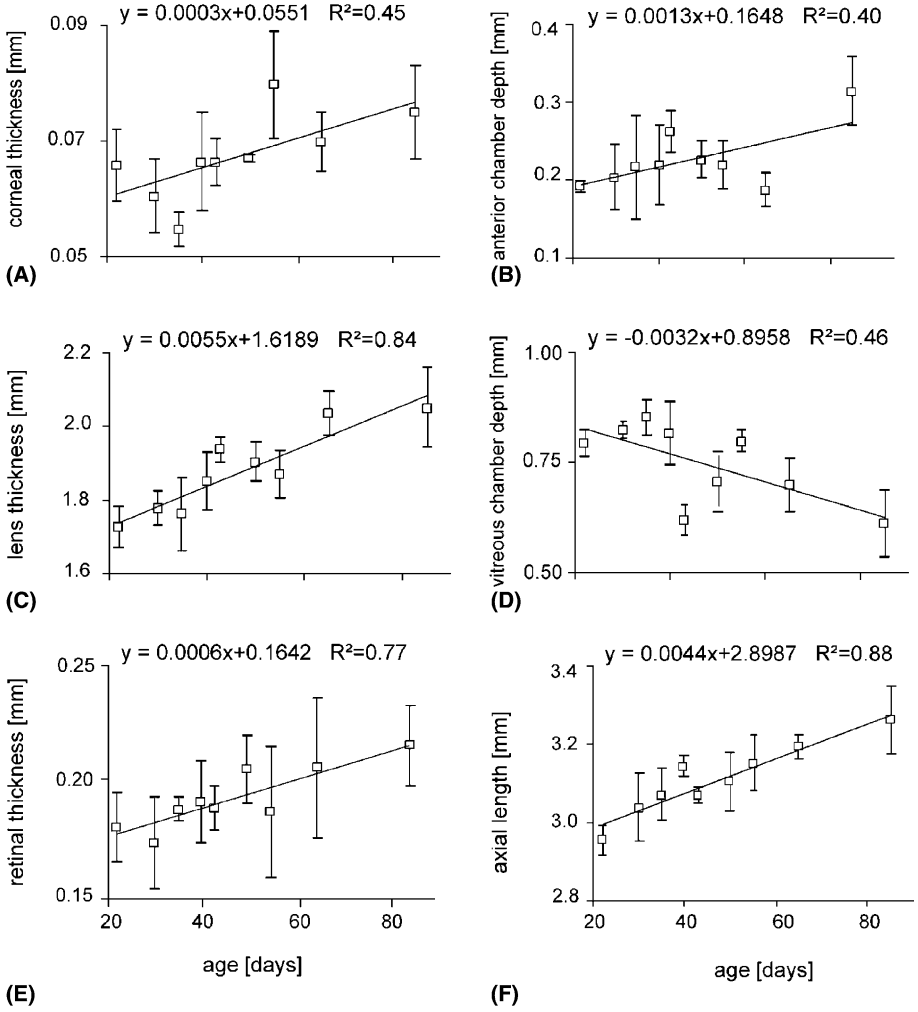

Fig. 5. Development of the ocular dimensions of the mouse eye between day 22 and 100. Axial length (F) is the sum of corneal thickness (A) + anterior chamber depth (B) + lens thickness (C) + vitreous chamber depth (D) + retinal thickness (E). Data are based on frozen sections from 34 eyes ($n = 3$ or more eyes for each data point). Error bars denote standard deviations.

anterior chamber depth, lens thickness, vitreous chamber depth and retinal thickness) increased from 3.00 mm at day 22 to 3.34 mm at day 100 (Fig. 5F). Also the lens grew continuously in both axial and horizontal

dimensions (axial lens growth is plotted as "lens thickness"), at a constant rate of 5.5 μm/day. Since axial length grew only by 4.4 μm/day, the vitreous chamber depth declined with age. Fig. 5E shows that retinal thickness (as measured near the optic nerve head) grew from 0.176 mm at day 22 to 0.223 mm at day 100, that is equivalent to a growth rate of 0.6 μm/day. Retinal thickness was comparable in human and mice which is in line with a notion of Glickstein and Millodot (1970) that retinal thickness is similar among different species of mammals, no matter of the absolute eye size.

The growth of the radii of curvature of the optical surfaces in the eye is shown in Fig. 6. Neither the anterior nor the posterior radius of corneal curvature changed significantly with age (Fig. 6A and B). The averaged radii from all measurements of the anterior surface were 1.414 ± 0.019 mm, and for the posterior surface 1.415 ± 0.044 mm. Photokeratometry in vivo gave a slightly flatter anterior surface of the cornea of 1.493 ± 0.080 mm. The difference was significant due to the large number of samples ($df = 66$, $T = 5.6$, $p < 0.001$, unpaired t-test). The larger standard deviation in the in vivo measurements reflects the difficulties in aligning the pupil axis of the mouse eye. It was noted that, if a Purkinje reflex was positioned close to the pupillary margin (due to inherent difficulties in centering), a flatter cornea was measured. This observation is in agreement with findings by Remtulla and Hallett (1985) and suggests an aspherical shape of the cornea and it could also explain that the averaged radii of curvature measured with photokeratometry were larger than with frozen sections. However, both techniques had in common that no changes were detected with age. Different from the cornea, the radii of curvature of the anterior lens surface increased with age from 0.982 mm at day 22 to 1.208 mm at day 100 (Fig. 6C). The posterior lens showed no significant change in shape if linear regression analysis was used (Fig. 6D). The radius of curvature of the anterior and posterior retinal surface did also not change significantly with age (Fig. 6E and F) with an average radius of curvature of the vitreo-retinal interface of -1.522 ± 0.033 mm and of the retinal pigment epithelium of -1.607 ± 0.030 mm.

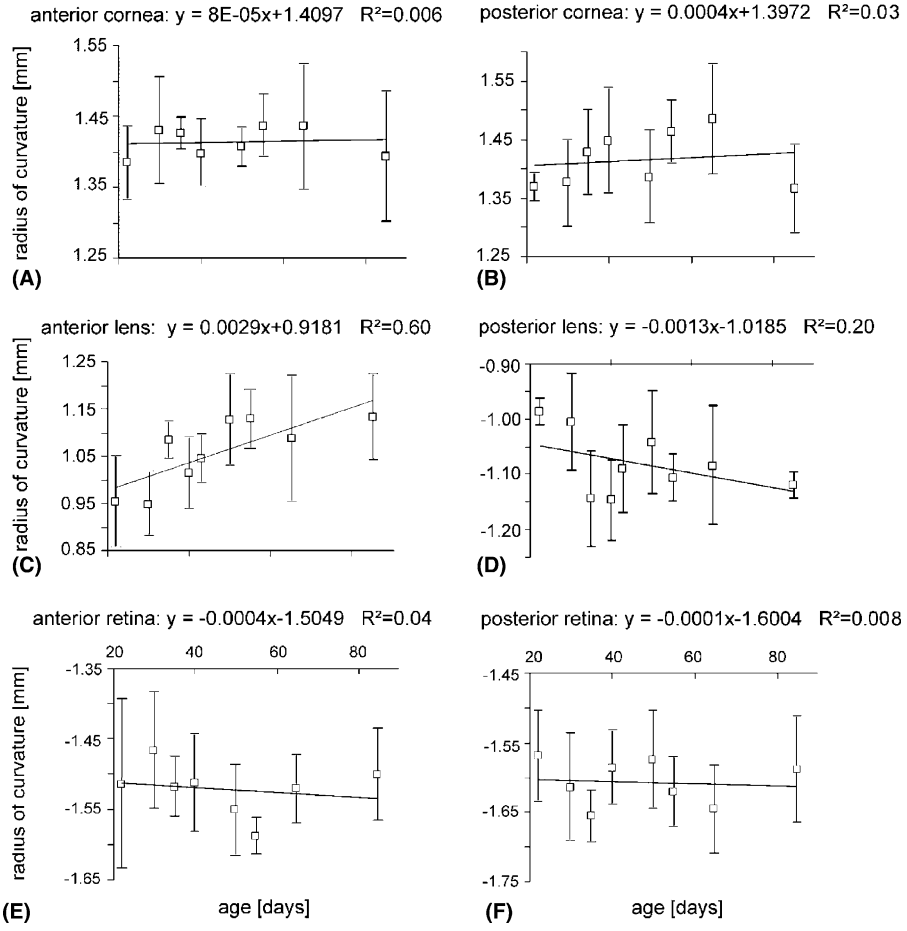

Fig. 6. Development of the radii of curvature of the anterior and posterior surface of the cornea (A,B), lens (C,D) and retina (E,F), as determined in frozen sections. Error bars denote standard deviations.

3.3. Schematic eye modelling

Using the regression analyses shown in Figs. 5 and 6, and the measured refractions shown in Fig. 2A, a schematic eye for the age range from 22 to 100 days was developed. The dynamic eye model allowed us to construct schematic eyes for all ages between these age limits. The first finding was that equivalent lens index was remarkably high and also had to increase linearly with age from 1.568 to 1.605 to reproduce the measured refractions (Fig. 7A).

The small eye artifact was calculated as the dioptric difference between the vitreo-retinal interface and the retinal pigment epithelium. It ranged from +35.2 to +39.1 D over the age range considered (Fig. 7B). It was also calculated how much the eye had to elongate to become one diopter more myopic (Fig. 7C). An elongation of 5.4 μm was necessary in a 22-day-old mouse and 6.5 μm was required for the refractive change in a 100-day-old mouse.

3.4. Image magnification and *f*/number

As in other studies (Hughes, 1977), the posterior nodal distance (PND) and hence image magnification were highly correlated with axial length (Fig. 8A). The ratio of PND to axial length provides a further variable that can determine image size at a given eye size (Ott & Schaeffel, 1995). In the schematic eye of the mouse, this ratio changed only little with age (Fig. 8B; from 0.603 to about 0.581). Therefore, the developmental increase in retinal image magnification of about 10%, from 31 μm/deg in young mice to 34 μm/deg in adult mice (Fig. 8C) results largely from scaling.

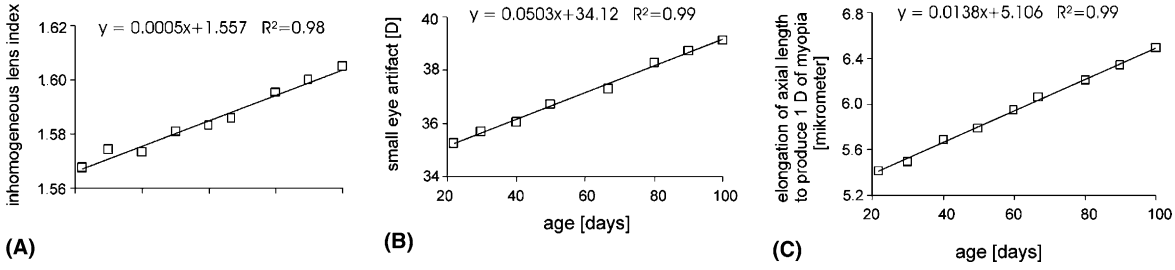

Fig. 7. (A) The refractive index of the growing lens was adjusted so that the schematic eye matched the refractive state measured by infrared photoretinoscopy. (B) The magnitude of the small eye artifact (Glickstein & Millodot, 1970) was calculated from the focal length and retinal thickness. (C) Axial elongation necessary to make the model eyes 1 D more myopic, as a function of age.

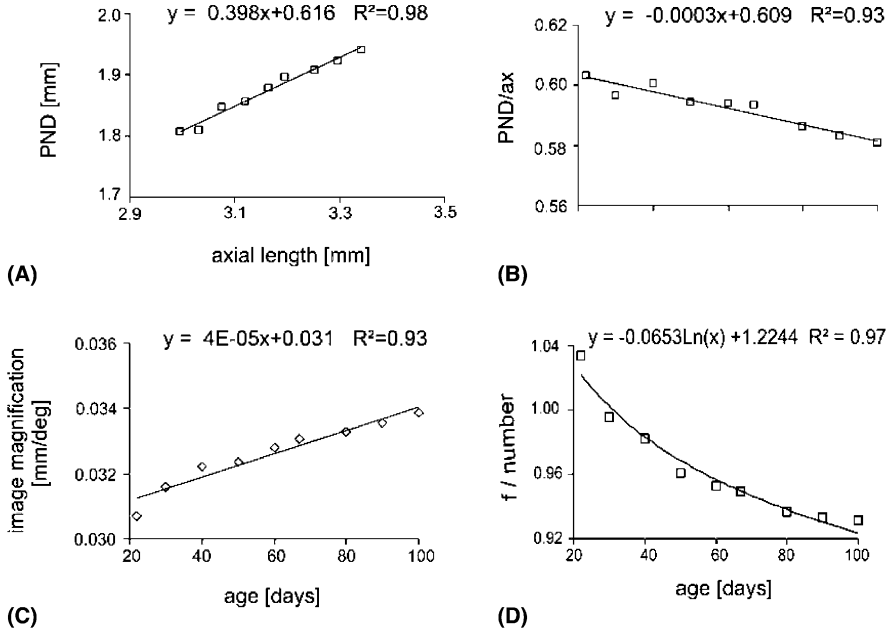

Fig. 8. (A) Posterior nodal distance (PND) was highly correlated with axial length. (B) The ratio of PND to axial length decreased with age and was slightly smaller than in most vertebrates (on average: 0.6, Hughes, 1977). (C) Retinal image magnification as a function of age. (D) The *f*/number declined during development resulting in a 10% brighter image at day 100 than at day 22. In this case, a logarithmic fit provided the best description of the data.

The size of the entrance pupil, as measured in vivo, was 1.75 mm at day 22 resulting in a f/number of 1.033 (Fig. 8D). The f/number declined slightly with age, resulting in a 10% brighter image at day 100 than at day 22. This change is less than in the chick (50 versus 1 day of age: +49%, Schaeffel, Howland, & Farkas, 1986), toad (adult toad versus tadpole: +350%, Mathis, Schaeffel, & Howland, 1988) or barn owl (60 versus 10 days: +30%, Schaeffel & Wagner, 1996). However, with a f/number $\leqslant 1.0$, the retinal image in the mouse eye is probably among the brightest of all vertebrates.

4. Discussion

4.1. Developmental stages

This study provides new data on refractive development and growth patterns in the mouse eye. In general, mice are weaned at three weeks of age (Sundberg, Smith, & John, 2002). They do not open their eyelids before 12–14 days postnatal (Sundberg et al., 2002) and the age of sexual maturity reached between 40 and 60 days (Zhou & Williams, 1999b). Decline in fecundity takes place between six and eight months of age and progressive changes of ageing develop from 12 months to the time of natural death at approximately 99 weeks (Sundberg et al., 2002).

4.2. Refractive state and small eye artifact

Refractive state seems to reach a constant value of approximately $+7.0 \pm 2.5$ D at the age of 70 days which could indicate that a stable refraction is reached only after sexual maturity. As in many other studies (i.e. Norton, Wu, & Siegwart, 2003), an unknown factor is the contribution of the small eye artifact. The true refraction of the mouse is likely to be more myopic than reported here. However, comparison of refractive state using both retinoscopy and visually evoked potentials in various animals (rat, Mutti, Ver Hoeve, Zadnik, & Murphy, 1997; pigeon, Millodot & Blough, 1971; ground squirrel, Gur & Sivak, 1979) suggests that the retinoscopic reflex may not simply arise from the vitreal–retinal interface because the small eye artifact should then be much larger and the animals, in fact, quite myopic. A new study (Norton et al., 2003) suggests that tree shrews which are measured with streak retinoscopy at +7.0 D and with an autorefractor (using infrared light) at about +4.0 D, are in fact about emmetropic when measured with visual evoked potentials. Thus, it is likely that the small amount of hyperopia measured with infrared photoretinoscopy in the mouse is also only a minor "small eye artifact". The reflecting layer(s) must be closer to the photoreceptor layer than assumed in the original paper on the small eye artifact (Glickstein & Millodot, 1970).

The refractive errors measured by infrared photoretinoscopy in the present study were less hyperopic than those reported by other authors in previous studies, in which white light streak retinoscopy was used. Tejedor and de la Villa (2003) found an apparent hyperopia of approximately +13.5 D in 30-day-old mice and Beuerman et al. (2003) found a refractive error of more than +15.0 D in adult Balb/CJ mice. A possible reason for this discrepancy is chromatic aberration which renders an eye more hyperopic in the red end of the spectrum. We have tested this hypothesis by replacing the infrared LEDs of the retinoscopy with yellow LEDs (peak emission at 550 nm). Cyclopleged mice were still not significantly more hyperopic. The average slope of the brightness profile in the pupil was 0.71 ± 0.24 (five measurements in one untreated animal), which converts into a refractive error of about +8.0 D. It is therefore also possible that the differences to previous studies can be attributed to the inherent difficulty to perform streak retinoscopy in an eye with a very small pupil. The mouse has a highly sensitive pupil response to light (Pennesi et al., 1998). Reliable measurements without cycloplegia at pupil sizes of 1 mm or even less appear demanding.

4.3. Growth rate

A striking feature of the mouse eye is its slow but long-lasting and linear growth rate between day 22 and 100. During this time, the lens grew at a rate of 5.5 μm/day and the globe at a rate of 4.4 μm/day. Zhou and Williams (1999b) examined eye weights in 507 mice from 50 different strains and also found that growth continued long after sexual maturity. In their study, the eye weight data could be best fit by linear regression when they were plotted versus the logarithm of age. There are also data on prenatal eye growth in the CD-1 mouse (E8 to E19), measured by ultrasound biomicroscopy (Foster, Zhang, Duckett, Cucevic, & Pavlin, 2003). Already before birth, the globe and the lens appear to grow linearly at a rate of 122 and 68 μm/day, respectively. At birth, the axial length should then be about 1.32 mm, about 40% of the value at 100 days. When the mice are weaned (around day 22), the globe has already reached about 90% of its size at 100 days, and 95% when sexual maturity is reached. The growth pattern in the mouse eye is similar to other species where also a period of rapid axial growth during early infancy (in mice: form birth to approximately day 22), is followed by a period of slower growth when the animals become juvenile (rhesus monkey, Bradley, Fernandes, Lynn, Tigges, & Boothe, 1999; marmoset, Graham & Judge, 1999; tree shrew, Norton & McBrien, 1992; chick, Irving, Sivak, Curry, & Callender, 1996). Also the human eye shows a biphasic growth curve (Gordon & Donzis, 1985; Larsen,

1971a). However, in comparison to the chick and tree shrew, the relative elongation of the mouse eye is approximately five times less. Between day 22 and 46, the mouse eye grew approximately 0.11 mm (~3.5%). The chicken eye elongated approximately 1.80 mm (~19%) over the same time period (Schaeffel & Howland, 1988). In the tree shrew, the eye grows more like in the chicken, about 19% over the same age range.

4.4. Growth of the ocular dimensions

In 22-day-old mice, corneal radius of curvature had almost reached its final value. Such early completion of corneal development has also been observed in cats (Thorn, Gollender, & Erickson, 1976), three shrews (Norton & McBrien, 1992) and humans (Oyster et al., 1999). Different from corneal curvature, anterior chamber of the mouse eye increased steadily with age (between day 22 and 100: 1.3 μm/day). This is similar in macaques (Kiely et al., 1987) marmosets (Graham & Judge, 1999), tree shrews (Norton & McBrien, 1992) and humans (Larsen, 1971b). A developmental decline in vitreous chamber depth due to prominent growth of the lens has, to our knowledge, been described only once before in the tree shrew eye (Norton & McBrien, 1992). That the lens grows continuously over the life span is common (i.e. tree shrews, Norton & McBrien, 1992; and kittens, Thorn et al., 1976). Also in humans, the lens continues to grow during adulthood (Cook, Koretz, Pfahnl, Hyun, & Kaufman, 1994) although there is a phase in late childhood between the age of 6 and 10 years (Zadnik, Mutti, Fusaro, & Adams, 1995), where the lens actually thins. It is not known whether it also reduces its volume.

Remtulla and Hallett (1985) analyzed 41 eyes from C57BL/6J mice between 98 and 203 days and described no age related changes of the optical components. In this study, corneal thickness (0.093 mm) and anterior chamber depth (0.452) were slightly larger compared to the values of 100-day-old mice in the present study (0.085 and 0.293 mm, respectively). Furthermore, Remtulla and Hallett (1985) described a thinner lens for adult mice (2.032 mm). However posterior chamber depth (0.558 mm; 100-day-old mouse: 0.572) and total axial length (3.372 mm; 100-day-old mouse: 3.339) were nearly equal in both studies. These minor differences trace most probably back to strain differences or differences in the rearing conditions.

4.5. Homogeneous lens index

The presence of a refractive index gradient in the lens is common to all vertebrate eyes (Campbell, 1984) but its structure is difficult to describe in detail (Acosta, Vazquez, Smith, & Garner, 2003), in part because it is variable among individual eyes (Artal, Berrio, Guirao, & Piers, 2002). In the present study, the description of the lens had to be confined to the paraxial region and no attempt was made to study the structure of the gradient index. It is clear that the equivalent homogeneous index is only a theoretical number which is much higher than what is biologically possible. However, the equivalent homogeneous indices in this study match the values found in other studies (chicken, Pickett-Seltner, Weerheim, Sivak, & Pasternak, 1987; Schaeffel & Howland, 1988). Also in the only published paraxial schematic eye model of the adult mouse (Remtulla & Hallett, 1985), the equivalent refractive index of 1.659 is in agreement with our findings.

4.6. Retinal image magnification and brightness

The difference in retinal magnification between a 22- and 100-day-old mouse was only about 10% but this value matches the changes expected from axial eye growth. The image magnification found in the 22-day-old mouse eye (31 μm/deg) was in agreement with the value that was previously published for adult mice (31 μm/deg at 550 nm, Remtulla & Hallett, 1985). This agreement is due to the paraxial focal length which matches the value for young mice in the present study.

In our study, the f/number of the adult mouse eye (0.93) was much lower than in humans (about 4.5, Schaeffel & Wagner, 1996), diurnal birds (60-day-old chick: 1.35, Schaeffel et al., 1986; pigeon: 1.98, Marshall, Mellerio, & Palmer, 1973) or in nocturnal birds (barn owl: 1.13, Schaeffel & Wagner, 1996). Hence, mice may have the brightest retinal images among vertebrates.

4.7. Depth of focus

The depth of focus has not been evaluated in this study. Remtulla and Hallett (1985) estimated that it may be as large as ±56 D, based on their eye size and photoreceptor diameter. They also had doubts that the behavioral depth of field can be as large since, for example in the rat eye, behavioral acuity can be five times higher than reported ganglion-cell acuity (Birch & Jacobs, 1979). This would reduce depth of field to ±11 D. Mice also seem to lack the ciliary muscle (Woolf, 1956) and are assumed to be unable to accommodate (Artal, Herreros de Tejada, Munoz Tedo, & Green, 1998) which is compatible with the existence of an appreciable depth of field. Thus, small refractive errors may not be so critical in mouse eyes.

4.8. Deprivation myopia

The mouse eye turned out to be a demanding model in which to study deprivation myopia (Schaeffel et al., 2004; Tejedor & de la Villa, 2003). Degrading the retinal image with diffusers or lid-suture induced a shift in

refractive state in the myopic direction but the anatomical correlate, an increase in axial length, was unconvincing (Schaeffel & Howland, 2003). Assuming that the dioptric amount of myopia that can be induced depends on the natural dioptric growth rate of the eye, 0.8 D of myopia could be induced per day in a 22-day-old mouse. Since the dioptric growth rate declines with age (from 0.80 D at day 22 to 0.68 D at day 100), an occlusion period of at least 12 days is necessary to produce approximately 10 D of myopia, equivalent to a change of axial length of 55 μm. Compared to other animal models, the mouse eye shows a smaller dioptric growth rate per day. A 20-day-old chick grows approximately −1.75 D/day (Schaeffel & Howland, 1988). Troilo and Judge (1993) suggested a dioptric growth rate of −1.25 D/day in the 20-day-old marmoset. However, in these animals the growth rate levels off more rapidly. In the chicken eye, it is less than −0.5 D at day 80 post-hatching and the marmoset eye has already stopped growing.

In conclusion, one of the reasons why the mouse eye is a challenging model of myopia is its relatively slow growth, making long treatment periods necessary to induce significant deprivation myopia. Further research is needed to determine whether the relatively poor optical quality (Artal et al., 1998) and the rod dominance in the retina may be other complicating factors.

Acknowledgements

This study was supported by the fortune program of the Medical Faculty of the University of Tuebingen. We are grateful to Howard C Howland for help with the OSLO ray tracing program, and for improving an earlier version of the manuscript.

References

Acosta, E., Vazquez, D., Smith, G., & Garner, L. (2003). A comparison and analysis of various techniques for determining the gradient index distribution of non-symmetric crystalline lenses. Available: http://research.opt.indiana.edu/Meetings/Mopane2003/Acosta/Acosta.pdf.

Artal, P., Berrio, E., Guirao, A., & Piers, P. (2002). Contribution of the cornea and internal surfaces to the change of ocular aberrations with age. *Journal of the Optical Society of America A, Optics, Image Science, and Vision, 19*, 137–143.

Artal, P., Herreros de Tejada, P., Munoz Tedo, C., & Green, D. G. (1998). Retinal image quality in the rodent eye. *Visual Neuroscience, 15*, 597–605.

Beuerman, R. W., Barathi, A., Weon, S. R., & Tan, D. (2003). Two models of experimental myopia in the mouse. *Investigative Ophthalmology and Visual Science, 44*(Suppl.), 4338.

Birch, D., & Jacobs, G. H. (1979). Spatial contrast sensitivity in albino and pigmented rats. *Vision Research, 19*, 933–938.

Bradley, D. V., Fernandes, A., Lynn, M., Tigges, M., & Boothe, R. G. (1999). Emmetropization in the rhesus monkey (*Macaca mulatta*): from birth to young adulthood. *Investigative Ophthalmology and Visual Science, 40*, 214–229.

Campbell, M. C. W. (1984). Measurement of refractive index in an intact crystalline lens. *Vision Research, 24*, 409–415.

Charman, W. N., & Tucker, J. (1973). Optical system of the goldfish eye. *Vision Research, 13*, 1–8.

Chaudhuri, A., Hallett, P. E., & Parker, J. A. (1983). Aspheric curvatures, refractive indices and chromatic aberration for the rat eye. *Vision Research, 23*, 1351–1364.

Cook, C. A., Koretz, J. F., Pfahnl, A., Hyun, J., & Kaufman, P. L. (1994). Aging of the human crystalline lens and anterior segment. *Vision Research, 34*, 2945–2954.

Fincham, W. H. A., & Freeman, M. H. (1974). *Optics* (8th ed.). London: Butterworth.

Foster, F. S., Zhang, M. Y., Duckett, A. S., Cucevic, V., & Pavlin, C. J. (2003). In vivo imaging of embryonic development in the mouse eye by ultrasound biomicroscopy. *Investigative Ophthalmology and Visual Science, 44*, 2361–2366.

Glickstein, M., & Millodot, M. (1970). Retinoscopy and eye size. *Science, 168*, 605–606.

Gordon, R. A., & Donzis, P. B. (1985). Refractive development of the human eye. *Archives of Ophthalmology, 103*, 785–789.

Graham, B., & Judge, S. J. (1999). Normal development of refractive state and ocular component dimensions in the marmoset *Callithrix jacchus*. *Vision Research, 39*, 177–187.

Gur, M., & Sivak, J. G. (1979). Refractive state of the eye of a small diurnal mammal: the ground squirrel. *American Journal of Optometry and Physiological Optics, 56*, 689–695.

Gwiazda, J., Hyman, L., Hussein, M., Everett, D., Norton, T. T., Kurtz, D., Leske, M. C., Manny, R., Marsh-Tootle, W., & Scheiman, M. (2003). A randomized clinical trial of progressive addition lenses versus single vision lenses on the progression of myopia in children. *Investigative Ophthalmology and Vision Science, 44*, 1492–1500.

Hughes, A. (1977). The topography of vision in mammals of contrasting life style: comparative optics and retinal organization. In F. Crescitelli (Ed.), *Handbook of sensory physiology* (Vol. VIII/5, pp. 613–756). Berlin, Heidelberg, New York: Springer.

Hughes, A. (1979). A schematic eye for the rat. *Vision Research, 19*, 569–588.

Irving, E. L., Sivak, J. G., Curry, T. A., & Callender, M. G. (1996). Chick eye optics: zero to fourteen days. *Journal of Comparative Physiology A, 179*, 185–194.

Kiely, P. M., Crewther, S. G., Nathan, J., Brennan, N. A., Efron, N., & Madigan, M. A. (1987). A comparison of ocular development of the cynomolgus monkey and man. *Clinical Visual Science, 1*, 269–280.

Kroger, R. H., Campbell, M. C., Fernald, R. D., & Wagner, H. J. (1999). Multifocal lenses compensate for chromatic defocus in vertebrate eyes. *Journal of Comparative Physiology A, 184*, 361–369.

Krumpaszky, H. G., Haas, A., Klauss, V., & Selbmann, H. K. (1997). New blindness incidents in Wurttemberg–Hohenzollern. *Ophthalmologe, 94*, 234–236 (in German).

Larsen, J. S. (1971a). The sagittal growth of the eye. III. Ultrasonic measurement of the posterior segment (axial length of the vitreous) from birth to puberty. *Acta Ophthamologica (Copenhagen), 49*, 239–262.

Larsen, J. S. (1971b). The sagittal growth of the eye. II. Ultrasonic measurement of the axial diameter of the lens and the anterior segment from birth to puberty. *Acta Ophthamologica (Copenhagen), 49*, 427–440.

Marshall, J., Mellerio, J., & Palmer, D. A. (1973). A schematic eye for the pigeon. *Vision Research, 13*, 2449–2453.

Mathis, U., Schaeffel, F., & Howland, H. C. (1988). Visual optics in toads (*Bufo americanus*). *Journal of Comparative Physiology A, 163*, 201–213.

Millodot, M., & Blough, P. (1971). The refractive state of the pigeon eye. *Vision Research, 11*, 1019–1022.

Mouse Genome Sequencing Consortium (2002). Initial sequencing and comparative analysis of the mouse genome. *Nature, 420*, 520–562.

Mutti, D. O., Ver Hoeve, J. N., Zadnik, K., & Murphy, C. J. (1997). The artifact of retinoscopy revisited: comparison of refractive error measured by retinoscopy and visual evoked potential in the rat. *Optometry and Vision Science, 74*, 483–488.

Norton, T. T., & McBrien, N. A. (1992). Normal development of refractive state and ocular component dimensions in the tree shrew. *Vision Research, 32*, 833–842.

Norton, T. T., Wu, W. W., & Siegwart, J. T., Jr. (2003). Refractive state of tree shrew eyes measured with cortical visual evoked potentials. *Optometry and Vision Science, 80*, 623–631.

Ott, M., & Schaeffel, F. (1995). A negatively powered lens in the chameleon. *Nature, 373*, 692–694.

Oyster, C. W. (1999). *The human eye: structure and function*. Sunderland, MA: Sinauer Associates.

Pacella, R., McLellan, J., Grice, K., Del Bono, E. A., Wiggs, J. L., & Gwiazda, J. E. (1999). Role of genetic factors in the etiology of juvenile-onset myopia based on a longitudinal study of refractive error. *Optometry and Vision Science, 76*, 381–386.

Pennesi, M. E., Lyubarsky, A. L., & Pugh, E. N. (1998). Extreme responsiveness of the pupil of the dark-adapted mouse to steady retinal illumination. *Investigative Ophthalmology and Visual Science, 39*, 2148–2156.

Pickett-Seltner, R. L., Weerheim, J., Sivak, J. G., & Pasternak, J. (1987). Experimentally induced myopia does not affect post-hatching development of the chick lens. *Vision Research, 27*, 1779–1783.

Rajan, U., Saw, S.-M., Lau, C., O'Brien, L., Chan, T.-K., Lam, D. S. C., & Chew, S.-J. (1998). Prevalence of myopia in schoolchildren and risk factors for its progression. In T. Tokoro (Ed.), *Myopia updates* (pp. 69–80). Tokyo, Berlin, Heidelberg, New York: Springer.

Remtulla, S., & Hallett, P. E. (1985). A schematic eye for the mouse and comparison with the rat. *Vision Research, 25*, 21–32.

Saw, S. M. (2003). A synopsis of the prevalence rates and environmental risk factors for myopia. *Clinical and Experimental Optometry, 86*, 289–294.

Schaeffel, F., & Burkhardt, E. (2002). Measurement of refractive state and deprivation myopia in the black wildtype mouse. *Investigative Ophthalmology and Visual Science, 43*(Suppl.), 182.

Schaeffel, F., Burkhardt, E., Howland, H. C., & Williams, R. W. (2004). Measurement of refractive state and deprivation myopia in two strains of mice. *Optometry and Vision Science, 81*, 99–110.

Schaeffel, F., & Howland, H. C. (1988). Visual optics in normal and ametropic chickens. *Clinical Vision Science, 3*, 83–98.

Schaeffel, F., & Howland, H. C. (2003). Axial length changes in myopic mouse eyes. *Investigative Ophthalmology and Visual Science, Electronic Letter* (April 25), 2003.

Schaeffel, F., Howland, H. C., & Farkas, L. (1986). Natural accommodation in the growing chicken. *Vision Research, 26*, 1977–1993.

Schaeffel, F., Simon, P., Feldkaemper, M., Ohngemach, S., & Williams, R. W. (2003). Molecular biology of myopia. *Clinical and Experimental Optometry, 86*, 295–307.

Schaeffel, F., & Wagner, H. (1996). Emmetropization and optical development of the eye of the barn owl (*Tyto alba*). *Journal of Comparative Physiology A, 178*, 491–498.

Sivak, J. G. (1974). The refractive error of the fish eye. *Vision Research, 14*, 209–213.

Sundberg, J. P., Smith, R. S., & John, S. W. M. (2002). Selection of controls. In R. S. Smith (Ed.), *Systematic evaluation of the mouse eye: Anatomy, pathology and biomethods* (pp. 77–80). Boca Raton, FL: CRC Press.

Tejedor, J., & de la Villa, P. (2003). Refractive changes induced by form deprivation in the mouse eye. *Investigative Ophthalmology and Visual Science, 44*, 32–36.

Thorn, F., Gollender, M., & Erickson, P. (1976). The development of the kitten's visual optics. *Vision Research, 16*, 1145–1150.

Thorn, F., Grice, K., Held, R., & Gwiazda, J. (1998). Myopia: nature, nurture, and the blur hypothesis. In L. L.-K. Lin, Y.-F. Shih, & P. T. Hung (Eds.), *Myopia updates II* (pp. 89–93). Tokyo, Berlin, Heidelberg, New York: Springer.

Troilo, D., & Judge, S. J. (1993). Ocular development and visual deprivation myopia in the common marmoset *Callithrix jacchus*. *Vision Research, 33*, 1311–1324.

Woolf, D. (1956). A comparative cytological study of the ciliary muscle. *Anatomical Record, 124*, 145–163.

Wu, S. Y., Nemesure, B., & Leske, M. C. (1999). Refractive errors in a black adult population: the Barbados eye study. *Investigative Ophthalmology and Vision Science, 40*, 2179–2184.

Young, T. L., Ronan, S. M., Drahozal, L. A., Wildenberg, S. C., Alvear, A. B., Oetting, W. S., Atwood, L., Wilkin, D. J., & King, R. A. (1998). Evidence that a locus for familiar high myopia maps to chromosome 18p. *American Journal of Human Genetics, 63*, 109–119.

Zadnik, K., Mutti, D. O., Fusaro, R. E., & Adams, A. J. (1995). Longitudinal evidence of crystalline lens thinning in children. *Investigative Ophthalmology and Visual Science, 36*, 1581–1587.

Zhou, G., & Williams, R. W. (1999a). Eye1 and Eye2: gene loci that modulate eye size, lens weight, and retinal area in the mouse. *Investigative Ophthalmology and Visual Science, 40*, 817–825.

Zhou, G., & Williams, R. W. (1999b). Mouse models for the analysis of myopia: an analysis of variation in eye size of adult mice. *Optometry and Vision Science, 76*, 408–418.